Spin-orbit term in the nuclear shell model

H. Müther ●*

Institut für Theoretische Physik, Universität Tübingen, Auf der Morgenstelle 14, D-72076 Tübingen, Germany

Quasinuclear systems, representing nuclei with variable size, are studied to investigate the occurrence of the spin-orbit term in the nuclear mean field in the transition from infinite nuclear matter to finite nuclei. Relativistic as well as nonrelativistic mean-field calculations based on models for the nucleon-nucleon (NN) interaction, which fit the NN scattering data, are considered. A very strong correlation between the strength of the spin-orbit term and radius of the nuclear system is observed. The origin of the spin-orbit term is analyzed by inspecting the contributions of the different partial waves and various mesons in a one-boson-exchange model of the NN interaction. Also results for a realistic interaction model based on chiral effective field theory including the contribution of three-nucleon interactions are discussed. The influence of correlation effects and the enhancement of the small component of Dirac spinors for nucleons in the nuclear medium are discussed.

I. INTRODUCTION

The nuclear shell model, which describes the nucleus as a system of protons and neutrons moving independently in a mean field generated by the interaction with all other nucleons, is the starting point of essentially all microscopic nuclear structure studies [1]. A rather strong spin-orbit term is an important ingredient of the nuclear mean field. Only after Goeppert Mayer [2] and Haxel, Jensen, and Suess [3] had suggested to incorporate such a spin-orbit term in the phenomenological Hamiltonian for the nuclear mean field, they were able to reproduce the empirical magic numbers, which occur in systematic studies of binding energies and nucleon separation energies.

This spin-orbit term is not only required to describe binding energies and separation energies, it is also an important part of the optical model potential for nucleon-nucleus scattering [4,5] and is a dominant feature in all microscopic studies of nuclear spectroscopy. As an example I mention the role of the spin-orbit term in suppressing the proton-neutron pairing in nuclei [6,7].

Such a spin-orbit term is a special attribute of many-body systems of finite size and cannot be extracted, e.g., from studies of infinite nuclear matter, which is frequently considered as a benchmark for microscopic nuclear structure studies. Therefore the spin-orbit term is often added to the nuclear mean field or a term is added to the phenomenological nucleon-nucleon (NN) interaction which generates a corresponding spin-orbit term in Hartree-Fock calculations as it is done, e.g., in the Skyrme forces [8].

The spin-orbit term is generated in a natural way in relativistic mean-field approaches as, e.g., in the so-called Walecka model [9,10]. A characteristic feature of such

relativistic models is the self-energy for the nucleons, which contains a large attractive component U_s, which transforms like a scalar under Lorentz transformation. In the evaluation of the single-particle energy of the nucleons this attractive contribution is compensated to a large extent by a repulsive component U_0, which behaves like the zero component of a Lorentz vector. If one reduces the corresponding Dirac equation, describing the single-particle properties of nucleons in a spherical nucleus, to a Schrödinger equation, one obtains a spin-orbit term, which can reproduce the empirical data of nuclei (see more detailed discussion below).

But also nonrelativistic studies of nuclei based on realistic models for the NN interaction, i.e., models which describe the experimental data of NN scattering, provide reasonable predictions for the spin-orbit structure of the nuclear mean field. In this case it is the spin structure of the two-body interaction which leads to the spin-orbit term in the single-particle spectrum of nuclei.

The main aim of the studies presented in this paper is to investigate and compare the predictions of relativistic and nonrelativistic approaches for the spin-orbit term in the nuclear mean field of light nuclei ($A \leqslant 56$). Special attention will be paid to the dependence of the spin-orbit term on the size of the nucleus by investigating spherical quasinuclear systems as a function of their radius. The studies are based on realistic one-boson-exchange (OBE) models for the NN interaction developed by Machleidt [11]. Effects of the different partial waves of the NN interaction as well as the influence of the different mesons considered in the OBE model on the structure of closed- and open-shell nuclei will be discussed. For a comparison an interaction model based on chiral effective field theory including terms up to fourth order in the chiral expansion has been considered [12]. Effects of the corresponding chiral three-nucleon (3N) interaction, expressed in the form of a density-dependent effective NN interaction [13,14], have been investigated.

---

*herbert.muether@uni-tuebingen.de

024306-1

After this short introduction Sec. II will contain the discussion of approaches which keep track of a relativistic structure nucleon self-energy, while Sec. III is devoted to nonrelativistic approaches. A comparison of the various approaches is presented in Sec. IV, which also contains the conclusion of the studies.

II. RELATIVISTIC APPROACH

At first sight relativistic effects seem to be negligible in nuclear structure calculations. The binding energies of the nucleons are much smaller than the mass of the nucleon and the typical values for the kinetic energy of nucleons bound in nuclei indicate that the velocities of the nucleons are well below the speed of light. The reason for the popularity as well as the success of the relativistic approaches is the feature that the resulting self-energy for the nucleon contains a very attractive term U_s, which transforms like a scalar under a Lorentz transformation, and a term U_0 which must be treated like the zero component of a Dirac vector. Inserting these two components into a Dirac equation for a nucleus with spherical symmetry leads to

$$\{\vec{\alpha} \cdot \vec{p} + \gamma_0[M + U_s(r)] + U_0(r)\}\Psi_\nu = \varepsilon_\nu \Psi_\nu, \qquad (1)$$

where I assume that U_s and U_0 are local and depend on the radial coordinate r. The Dirac spinors Ψ_ν can be written in the form

$$\Psi_\nu(\mathbf{r}) = \begin{pmatrix} g_\nu(r) \\ -if_\nu(r)\sigma \cdot \hat{\mathbf{r}} \end{pmatrix} \mathcal{Y}_{\kappa_\nu m_\nu}(\Omega)$$
$$= \begin{pmatrix} g_\nu(r)\mathcal{Y}_{\kappa_\nu m_\nu}(\Omega) \\ if_\nu(r)\mathcal{Y}_{-\kappa_\nu m_\nu}(\Omega) \end{pmatrix}. \qquad (2)$$

All quantum numbers of the states are expressed in terms of the index ν, which represents a radial quantum number n_ν, the projection quantum number for the total angular momentum m_ν, and the quantum number

$$\kappa_\nu = (2j_\nu + 1)(l_\nu - j_\nu),$$

representing the angular momenta. Note, that I am suppressing the isospin quantum numbers. As I am considering light nuclei with equal number of protons and neutrons and ignoring the effects of the Coulomb interaction, results are identical for protons and neutrons. The upper and lower spinor components in Eq. (2) have different orbital angular momenta l and I introduce the corresponding orbital angular momentum l'_ν for the same total angular momentum by

$$l'_\nu = \begin{cases} l_\nu + 1 & \text{for } l_\nu = j_\nu - 1/2 \\ l_\nu - 1 & \text{for } l\nu = j_\nu + 1/2 \end{cases}$$

and $\kappa'_\nu = -\kappa_\nu$. The spherical harmonics $Y_{lm}(\Omega)$ and the Pauli spinors are coupled to form

$$\mathcal{Y}_{\kappa_\nu m_\nu} = \sum_{m_l, m_s} C(l_\nu m_l, 1/2m_s | j_\nu m_\nu) Y_{l_\nu m_l}(\Omega) \chi_{1/2m_s}.$$

The Dirac equation (1) is solved by expanding the radial functions $g_\nu(r)$ and $f_\nu(r)$ in a discrete basis of spherical Bessel functions. The wave numbers for this basis are chosen such that this discrete basis is a complete orthonormal basis in a

sphere of radius D, which is chosen to be large enough that the results for the bound single-particle states are independent of D. With this expansion the Dirac equation is rewritten in the form of an eigenvalue problem and the eigenvalues ($\varepsilon_\nu = E_\nu + M$) and eigenvectors are determined by matrix diagonalization [15–17].

Instead of solving the Dirac equation one can also determine the solutions of positive energy by rewriting the two coupled equations of the Dirac equation (1) to form a Schrödinger equation:

$$\left[-\frac{\nabla^2}{2M} + V_{\text{cent}} + V_{ls}(r)\vec{\sigma} \cdot \vec{L} + V_{\text{Darwin}}(r)\right]\varphi_\nu(\mathbf{r})$$
$$= E_\nu \varphi_\nu(\mathbf{r}), \qquad (3)$$

where V_{cent}, V_{ls}, and V_{Darwin} represent the Schrödinger equivalent central, spin-orbit, and Darwin potentials, respectively. The potentials in Eq. (3) are obtained from the scalar U_s and vector U_0 potentials as

$$V_{\text{cent}} = U_s + \frac{\varepsilon}{M}U_0 + \frac{1}{2M}[U_s^2 - U_0^2],$$
$$V_{ls} = -\frac{1}{2MrD(r)}\frac{dD(r)}{dr},$$
$$V_{\text{Darwin}} = \frac{3}{8MD(r)}\left[\frac{dD(r)}{dr}\right]^2 - \frac{1}{2MrD(r)}\frac{dD}{dr}$$
$$- \frac{1}{4MD(r)}\frac{d^2D(r)}{d^2r}, \qquad (4)$$

where D is defined as

$$D(r) = M + \varepsilon + U_s(r) - U_0(r). \qquad (5)$$

The radial wave functions $\varphi_\nu(r)$ resulting from the Schrödinger equation (3) are related to the corresponding upper component of the Dirac spinors $\Psi_\nu(r)$ in (2) by

$$\varphi_\nu(r) \sim \frac{g_\nu(r)}{D(r)}.$$

One of the aims of the present paper is to investigate the occurrence of the spin-orbit term in the transition from nuclear matter to finite nuclei. For that purpose a set of "quasinuclear systems" has been constructed to exhibit this transition, e.g., for quasinuclear ^{16}O [7]. In this case a sequence of Woods-Saxon potentials

$$V_{\text{WS}}(r) = \frac{V_0}{1 + e^{(r-r_0)/a}}. \qquad (6)$$

Assuming a value of $a = 0.5$ fm for the surface width, the parameter for the depth of the potential V_0 has been adjusted in such a way that for different values of r_0 the energy of the first excited single-particle state with $l = 0$ occurred at zero energy. Occupying the corresponding $0s$ and $0p$ states with protons and neutrons one obtains a nuclear density distribution with root-mean-square radii $\langle r \rangle(r_0)$. These density distributions

$$\rho_{\langle r \rangle}(r), \qquad (7)$$

as well as the corresponding single-particle wave functions, have been used to explore the occurrence of the spin-orbit term due to the localization of the quasinuclear system ^{16}O.

In an analogous way quasinuclear systems for ^{40}Ca have been constructed. In this case the depth parameter V_0 in Eq. (6) has been adjusted to localize the $1p$ single-particle state at zero energy and $0s$, $0p$, $0d$, and $1s$ states have been occupied to obtain nuclear density distributions for ^{40}Ca with various radii.

As a first attempt the spin-orbit term has been evaluated using the improved local-density approximation (ILDA), which has recently been proposed by Sun *et al.* [18]. The ILDA is based on Dirac–Brueckner–Hartree-Fock (DBHF) calculations [19], which determine the relativistic components of the nucleon self-energy in nuclear matter

$$U_s^{\mathrm{NM}}(\rho, \beta, E) \quad \text{and} \quad U_0^{\mathrm{NM}}(\rho, \beta, E) \tag{8}$$

depending on the density ρ, the proton-neutron asymmetry β, and the nucleon energy E relative to the corresponding Fermi energy. Since only isospin symmetric systems will be considered here, the differences of the self-energy terms for protons and neutrons have been dropped and the limit of symmetric nuclear matter ($\beta = 0$) will be considered. The DBHF calculations are based on the Bonn potential [11] and use the subtracted T-matrix approach [19] to extract the relativistic components. A convenient parametrization of the self-energies of Eq. (8) has been presented in [18].

Using, e.g., the density profiles defined in Eq. (7) one can evaluate local self-energy components:

$$U_{s(0)}^{\mathrm{LDA}}(r, E) = U_{s(0)}^{\mathrm{NM}}(\rho(r), E). \tag{9}$$

The studies of Sun *et al.* [18] showed that this simple local-density approximation misses an important surface effect, which is due to the finite range of the interaction. Therefore they used an ILDA [20,21]:

$$U_{s(0)}^{\mathrm{ILDA}}(r, E) = \frac{1}{(t\sqrt{\pi})} \int U_{s(0)}^{\mathrm{LDA}}(r', E) \left\{ \exp\left[-\frac{(r-r')^2}{t^2}\right] \right.$$
$$\left. - \exp\left[-\frac{(r+r')^2}{t^2}\right] \right\} \frac{r'}{r} dr', \tag{10}$$

where t is an effective range parameter, which has been fitted to take values

$$t = 1.3528–0.1322A^{1/3} \quad [\mathrm{fm}], \tag{11}$$

depending on the mass number A of the nucleus under consideration.

Using the density distributions of Eq. (7) the corresponding U_s^{ILDA} and U_0^{ILDA} can easily be calculated and inserted into the Dirac equation (1) to obtain the resulting single-particle energies $E_\nu = \varepsilon_\nu - M$. Note that this must be done in an iterative way to obtain self-consistent solutions, for which the energy variable E in the self-energies $U_{s(0)}^{\mathrm{ILDA}}$ corresponds to the solutions E_ν of the Dirac equation. This energy dependence reflects the treatment of the NN correlations in the DBHF calculations, the basis of the ILDA approach.

Results for the spin-orbit splitting in quasinuclear systems with proton number $Z = 8$ and neutron number $N = 8$, i.e.,

quasinuclear ^{16}O, are presented in Fig. 1 as a function of the radius $\langle r \rangle$ of the nucleon density distribution $\rho_{\langle r \rangle}(r)$ of Eq. (7). The differences in the single-particle energies

$$\Delta E_{\mathrm{rel}} = E_{0p1/2} - E_{0p3/2}, \tag{12}$$

obtained from the solution of the Dirac equation, are represented by the black solid curve in the left panel of this figure, while corresponding results for the difference between the energies of the $d_{3/2}$ and $d_{5/2}$ shells are given in the right panel of Fig. 1.

The results displayed in this figure show a very strong dependence of the spin-orbit splitting on the radius of the underlying nucleon distribution. The spin-orbit splitting disappears for larger radii, which means it occurs only for sufficient localization of the nuclear structure. This effect is larger for the p shell than for the d shell, which represents states above the Fermi energy of ^{16}O.

In a complete self-consistent ILDA calculation [18] the nucleon density profile to determine the Dirac self-energies is determined from the resulting Dirac spinors. It is worth noting that the spin-orbit terms and radius of such a self-consistent calculation of ^{16}O, indicated by the blue triangles, denoted by "Dirac" in Fig. 1, are in line with the ILDA calculations using the various nuclear distributions derived from Woods-Saxon potentials. This supports the idea that the family of density distributions discussed above is a reasonable choice to explore the dependence of the spin-orbit term on the size of the nuclear system. One may also conclude, however, that the values of the spin-orbit splitting are not very sensitive to details of the density profile.

The experimental data for radius and spin-orbit splitting are represented by the black diamonds in Fig. 1. The calculations are in reasonable agreement with the experimental data. The calculated values for the spin-orbit splitting and/or the radius of nucleon distribution are slightly smaller than the experimental data. It is a well-known feature of DBHF calculations for finite nuclei that they tend to yield density profiles with too small radii [22]. This feature may be a bit enhanced in the present paper as the effects of the Coulomb repulsion between protons have been ignored.

In order to study the origin of the spin-orbit splitting in the framework of relativistic mean-field calculations, the transformation of the Dirac equation to the Schrödinger equation (3) has been considered and the expectation values of the spin-orbit potential (4),

$$\langle \varphi_\nu | V_{ls} | \varphi_\nu \rangle, \tag{13}$$

have been calculated. The results obtained from these expectation values are plotted as red dashed lines, identified as $\langle V_{ls} \rangle$ in Fig. 1. These results derived from the expectation values are very close to the results extracted from the Dirac single-particle energies (ΔE_{rel} in this figure). Therefore one may conclude that it is simply this spin-orbit term which determines the final spin-orbit splitting with high accuracy.

In detail, however, the situation is a bit more involved: If one determines the eigenstates of the single-particle Hamiltonian using the ILDA for the different nuclear distributions one obtains different radial wave functions for the states with
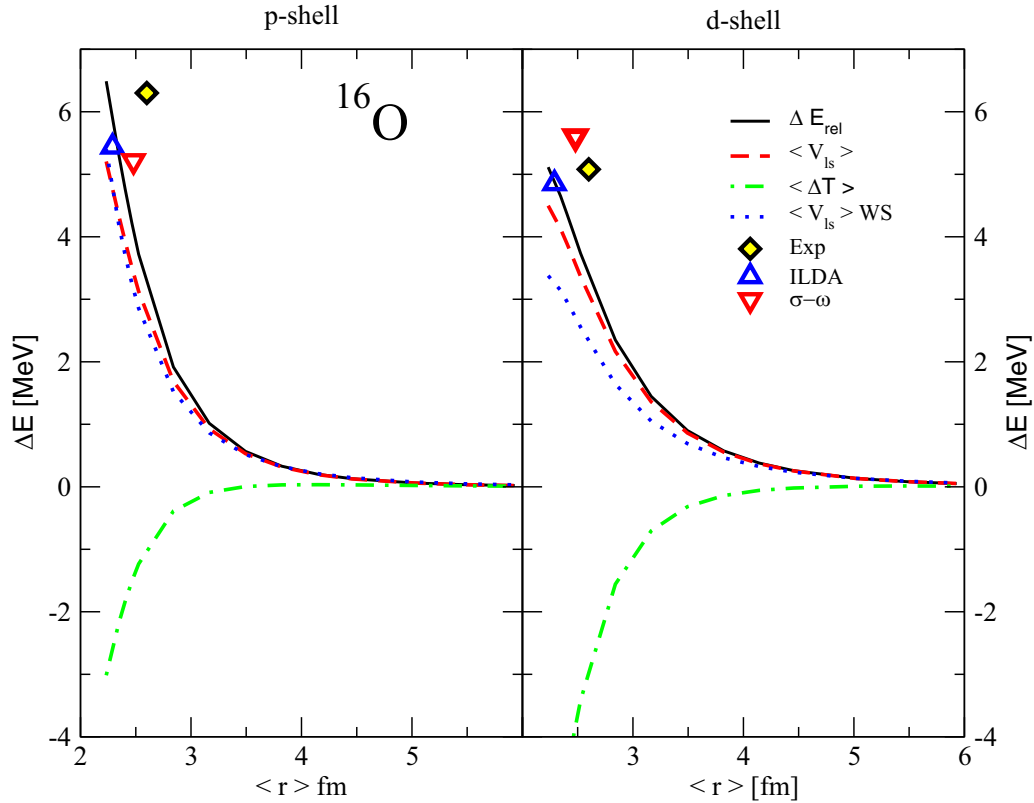
FIG. 1. Results for the spin-orbit splitting in quasinuclear ^{16}O are displayed as a function of the radius of the nucleon density distribution $\langle r \rangle$. The left panel presents results for the splitting in the p shell [see Eq. (12)] whereas the right panel shows corresponding results for the d shell. Further explanations are given in the text.

$j = l + 1/2$ and $l - 1/2$. The $j = l + 1/2$ state has a larger binding energy than the one with $j = l - 1/2$ and therefore is more localized, which leads to larger kinetic energy. This means that the difference of the corresponding expectation values for the kinetic energies,

$$\langle \Delta T \rangle = \langle T \rangle_{j=l-1/2} - \langle T \rangle_{j=l+1/2}, \tag{14}$$

is negative. The corresponding results are represented by green dash-dotted lines with label $\langle \Delta T \rangle$ in Fig. 1. It turns out that the absolute values of these differences are almost of the same size as the spin-orbit splitting due to Eq. (13). It is interesting to note that this effect in the kinetic energy is compensated with high accuracy by the difference in the expectation values for the central term and the Darwin term of the Hamiltonian, which leads to

$$\Delta E_{\text{rel}} \approx \langle V_{ls} \rangle, \tag{15}$$

observed in Fig. 1.

The blue dotted lines in this figure, labeled as $\langle V_{ls} \rangle$WS in the legend of the figure, represent the expectation value of the spin-orbit potential (4) using the wave functions of the Woods-Saxon potential (6), which has been used to generate the corresponding density distribution with radius $\langle r \rangle$. Note that the potential (6) is a pure central potential, which implies that the radial wave functions for the two spin-orbit states are identical. The results for $\langle V_{ls} \rangle$WS are close to the corresponding expectation values $\langle V_{ls} \rangle$ which were calculated using the eigenfunction of the single-particle Hamiltonian.

This indicates that expectation value $\langle V_{ls} \rangle$ is not very sensitive to details of the wave functions.

Figure 1 also shows results from two self-consistent calculations of ^{16}O, which are based on DBHF results of nuclear matter using two different local-density approximations. The ILDA approach [18] has been introduced above and the results for radius and spin-orbit splitting represented by a triangle with upward orientation have been mentioned above. The second approach has been defined in [16] extracting density-dependent coupling constants of a mean-field model with a scalar (σ) and vector meson (ω) to reproduce the Dirac components of the nuclear self-energy derived from DBHF calculations [23] of nuclear matter. The radius resulting from this $\sigma - \omega$ model (represented by a downward oriented triangle) is slightly larger than the ILDA prediction but also too small compared with experiment.

The spin-orbit potentials of Eq. (4) derived from these two self-consistent Dirac calculations are displayed in Fig. 2. One finds substantial differences for small r, which are not relevant in calculating expectation values for orbits with $l = 1$ and 2. The differences at the surface of the nucleus reflect the different radii and the fact that the $\sigma - \omega$ model yields a value for the spin-orbit splitting in the d shell, which is slightly larger as compared to the result evaluated within ILDA.

Results for the nucleus ^{40}Ca are displayed in Fig. 3 for the hole states of the $0d$ shell and the particle states of $1p$ and $0f$ shells. The conclusion drawn from the discussion of the results for ^{16}O, displayed in Fig. 1, is confirmed by inspecting
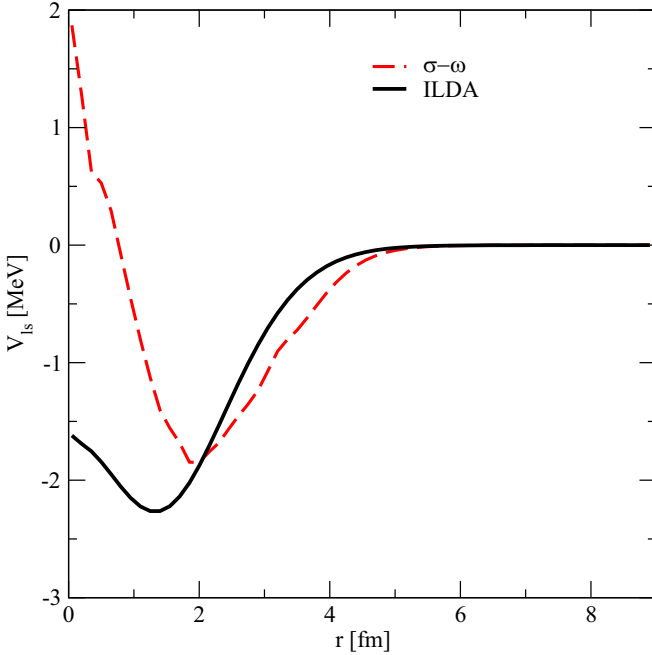
FIG. 2. Radial shape of the spin-orbit potential V_{ls} of Eq. (4). Results for ^{16}O are presented using the self-consistent ILDA approach (solid line) and the $\sigma - \omega$ model with density-dependent coupling constants derived from DBHF calculations [16].

the results for ^{40}Ca. The experimental data for spin-orbit splitting of the hole states are larger than the spin-orbit splitting for the particle states. This is nontrivial keeping in mind that $l\dot{s}$ is larger for the f shell than for the d shell. This trend of the experimental data is nicely reproduced by the self-consistent ILDA and $\sigma - \omega$ calculations and is also visible in study of density distributions of different radii.

The results for spin-orbit splittings in ^{16}O and ^{40}Ca derived from the self-consistent ILDA calculations as well as the $\sigma - \omega$ model using density-dependent coupling constants are also displayed in Table I. These results are complemented by results for nuclei with $N = Z$ and closed subshells: ^{12}C, ^{28}Si, and ^{56}Ni. Also these calculations have been performed assuming spherical symmetry. It should be noticed that the spin-orbit splitting derived from such calculations tends to predict larger values than derived from experimental data.

III. NONRELATIVISTIC STUDIES

The aim of this section is to discuss the spin-orbit term of the nuclear shell model within the framework of nonrelativistic many-body calculations based on realistic NN interactions. In this case the origin of the spin-orbit term should be related to the spin structure of the NN interaction, reflected in the spin dependence of the NN scattering phase shifts. Traditional models of realistic NN interactions like the local interactions of the Argonne group [24] or the various one-boson-exchange potentials (OBEPs) of the Bonn (Idaho) group [11,25,26] contain strong short-range and tensor components, which make it inevitable to employ nonperturbative approximation schemes for the solution of the many-nucleon system.

One way to get rid of the short-range or high-momentum components of such interactions is to use renormalization techniques [27–31] to separate low-momentum and high-momentum components of the NN interaction. For that purpose I consider the two-nucleon problem using the Bonn A interaction defined in [11] and define projection operators P and Q projecting on the subspace of two-nucleon states with momenta below a cutoff Λ and the complement, respectively. Using the unitary-model-operator approach [32] one can define a unitary transformation U in such a way that the transformed Hamiltonian does not couple the P and Q subspaces, which means

$$QU^{-1}HUP = 0, \tag{16}$$

with the original Hamiltonian $H = T + V$ containing the term for the kinetic energy T and the OBEP V. This leads to an effective Hamiltonian:

$$H_{\text{eff}} = T + V_{\text{low } k}, \tag{17}$$

with

$$V_{\text{low } k} = U^{-1}(T + V)U - T. \tag{18}$$

The eigenvalues, which are obtained by diagonalizing the effective Hamiltonian of (17) in the P space, are identical to those which are obtained in the diagonalization of the original Hamiltonian $H = T + V$ in the complete space. This implies that $V_{\text{low } k}$ yields the same NN phase shifts for nucleons with momenta below the cutoff Λ as the original OBE interaction V.

If the cutoff Λ is appropriately chosen, i.e., around $\Lambda = 2 \text{ fm}^{-1}$, the resulting low-momentum interaction $V_{\text{low } k}$ will describe the experimental data up to the pion threshold. Moreover, a very attractive aspect is that this $V_{\text{low } k}$ interaction turns out to be independent of the underlying realistic interaction V [29]. Uncertainties due to the different models of the high-momentum components of traditional realistic NN interaction have been removed by the renormalization procedure leading to $V_{\text{low } k}$.

With respect to the present paper it is a major advantage that $V_{\text{low } k}$ yields rather stable results in lowest-order many-body calculations. As will also be demonstrated below the results obtained in mean-field approximation are not very much modified including effects of correlations.

A major drawback in using $V_{\text{low } k}$ is the fact that it does not provide realistic saturation properties. Using $V_{\text{low } k}$, e.g., in a calculation of nuclear matter, one obtains a binding energy per nucleon increasing with density in a monotonic way [33]. Therefore three-nucleon forces have to be added to provide good results for the saturation of nuclear matter [28] and bulk properties of finite nuclei [34].

This is in line with the use of interaction models based on chiral perturbation theory [35,36]. Also these chiral interactions are limited to nucleons with low momenta and three-nucleon forces are required to reproduce the saturation properties of nuclear systems (see, e.g., the review [37] and references there). This point will be further discussed below.

The first approach to be discussed in this section is based on the Woods-Saxon wave functions generated to describe quasinuclear systems of varying size representing ^{16}O and
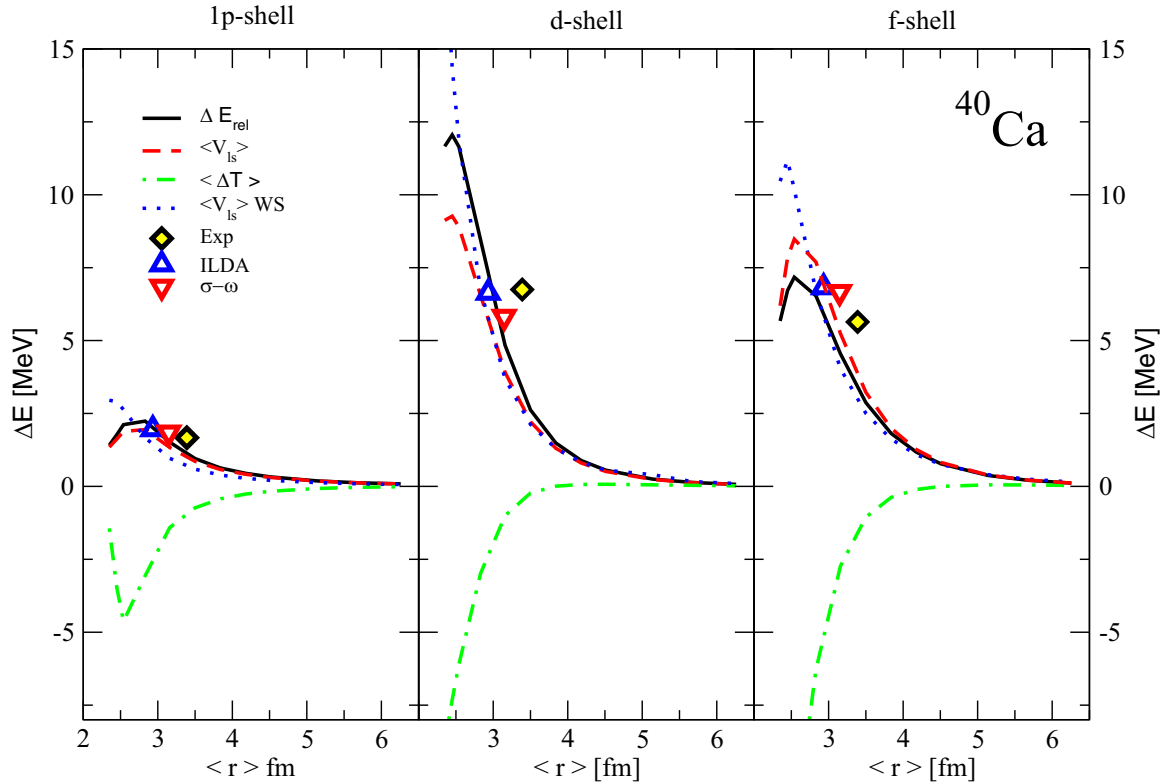
FIG. 3. Results for the spin-orbit splitting in quasinuclear ^{40}Ca are displayed as a function of the radius of the nucleon density distribution $\langle r \rangle$. The left, the middle, and the right panel present results for the splitting in the $1p$ shell, the $0d$ shell, and the $0f$ shell, respectively. The various approximations are discussed in the text (see also Fig. 1).

^{40}Ca [see Eq. (6)]. Denoting the eigenstates of the Woods-Saxon potential by $|\mu\rangle$ and $|\nu\rangle$ corresponding mean fields and single-particle energies

$$\varepsilon_\mu^{\text{WS}} = \langle \mu | T | \mu \rangle + \sum_{\nu < F} \langle \mu\nu | V_{\text{low } k} | \mu\nu \rangle \qquad (19)$$

can be calculated with the restriction of the summation on the right-hand side of this equation to states ν below the Fermi surface of the nucleus considered.

TABLE I. Spin-orbit splitting for various nuclei with closed shells or subshells calculated in various approximations (see first column and discussion in the text) assuming spherical symmetry. The shells under consideration are indicated in the second line. Experimental data for nuclei with closed subshells (numbers in brackets) have been derived from the spectrum of nuclei with one additional neutron. All entries are given in MeV.

	^{12}C	^{16}O		^{28}Si	^{40}Ca		^{56}Ni
	$0p$	$0p$	$0d$	$0d$	$0f$	$1p$	$0f$
Expt.	(2.83)	6.30	5.08	(0.80)	5.64	1.67	(2.23)
ILDA	4.18	5.44	4.85	5.85	6.83	1.96	6.79
$\sigma - \omega$	6.46	5.21	5.60	7.19	6.66	1.85	7.45
HF $+3N$	-2.34	3.91	4.57	-0.69	4.96	1.30	0.11
$m*$	0.25	5.48	6.11	1.74	6.66	1.59	2.30

It is worth noting that the Woods-Saxon wave functions are expanded in the same discrete basis of spherical Bessel functions, which has also been used for the solution of the Dirac equation discussed in the previous section. Since the effective interaction is evaluated in a basis of momentum eigenstates in partial waves of the relative basis one has to transform the matrix elements to the plane-wave states in the laboratory system using the vector brackets as described in [38,39]. This transformation is a bit more involved than the corresponding Talmi-Moshinsky transformation [40,41] to be used for a basis system of oscillator eigenstates.

Results for the spin-orbit splitting in the $0p$, $0d$, and $0f$ shell calculated from the energies of (19) are displayed in the various panels of Fig. 4 as a function of the radius of the quasinuclear system ^{16}O. The ls splittings using the wave functions of the corresponding Woods-Saxon potentials are represented by the solid black line using the label "WS $V_{\text{low } k}$." The results for the spin-orbit splitting depend very strongly on the radius of the quasinuclear system. This is very similar to the results obtained within the relativistic mean-field calculations discussed in the preceding section (see Fig. 1). For a given radius of the nucleon distribution, however, the results derived from relativistic mean-field calculations are typically around 30% smaller than the corresponding results evaluated from the NN interaction.

The results are rather insensitive to the details of the single-particle wave functions leading to the same radius for the nuclear system. If one replaces, e.g., the Woods-Saxon wave
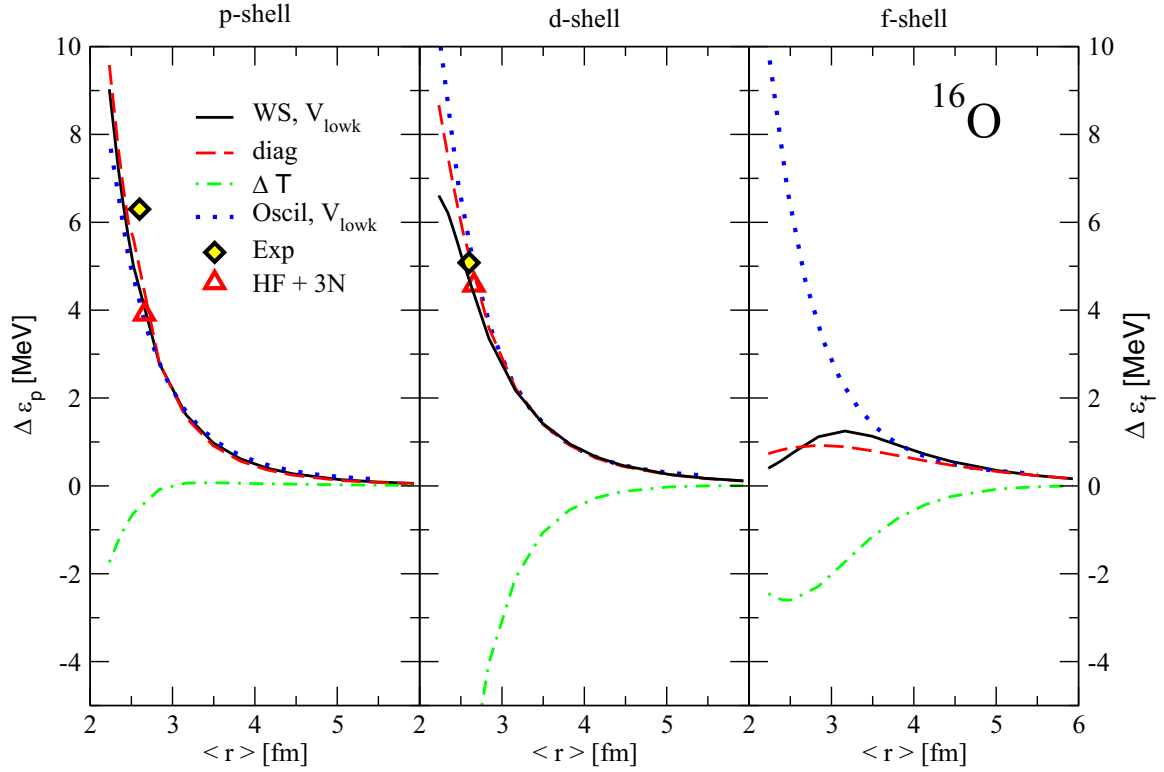
FIG. 4. Results for the spin-orbit splitting in quasinuclear ^{16}O are displayed as a function of the radius of the nucleon density distribution $\langle r \rangle$. The left, the middle, and the right panel present results for the splitting in the $0p$ shell, the $0d$ shell, and the $0f$ shell, respectively. The various approximations are discussed in the text.

functions in Eq. (19) by corresponding eigenfunctions of the harmonic oscillator with varying oscillator length, one obtains the results which are represented by the blue dotted lines (label "Oscil $V_{\text{low}\,k}$"), which, in the case of the $0p$ and $0d$ shell, are rather close to the results using Woods-Saxon wave functions. Differences occur in the case of the $0f$ shell. In this case the Woods-Saxon potential yields continuum states whereas the oscillator model generates bound states, which are not very realistic.

In order to test the sensitivity of the spin-orbit energy differences on details of the single-particle wave functions one may also consider the single-particle Hamiltonian

$$\langle \kappa | h | \nu \rangle = \langle \kappa | T | \mu \rangle + \sum_{\nu < F} \langle \kappa \nu | V_{\text{low}\,k} | \mu \nu \rangle, \qquad (20)$$

and derive the single-particle splitting from the eigenvalues of $\langle \kappa | h | \nu \rangle$. The results are shown in Fig. 4 as red lines with long dashes (label "diag"). In contrast to wave functions derived from the Woods-Saxon or oscillator model, these eigenstates yield different expectation values for the kinetic energies of the states of a spin-orbit doublet. In fact, the differences are non-negligible and provide negative contributions to the energy differences (see green dash-dotted lines in Fig. 4, label "ΔT"). This difference is counterbalanced by more attractive contributions of the central field in the case of $j = l + 1/2$ as compared to $j = l - 1/2$. Therefore the resulting spin-orbit splittings almost coincide with corresponding results using Woods-Saxon or oscillator states. This is very similar to the phenomenon displayed in Fig. 1 discussed above.

Figure 4 also displays results for spin-orbit splitting and nuclear radius obtained in a self-consistent Hartree-Fock (HF) calculation using $V_{\text{low}\,k}$. As it has already been mentioned above such Hartree-Fock calculations do not show saturation in infinite nuclear matter and predict finite nuclei with very small radii. Therefore the $V_{\text{low}\,k}$ interaction has been supplemented in [34] by a 3N force of zero range. leading to results for the saturation point of nuclear matter as well as radii and binding energies of light nuclei, which are in good agreement with the experimental data. Results for radius and spin-orbit splitting in ^{16}O from HF calculations using $V_{\text{low}\,k}$ supplemented by such a 3N force are represented by red triangles in Fig. 4. The results are rather close to the corresponding values using Woods-Saxon or oscillator functions leading to the same radius for the mass distribution.

The main conclusions resulting from this discussion of results for ^{16}O displayed in Fig. 4 are confirmed by corresponding results for ^{40}Ca presented in Fig. 5.

Results of HF calculations for spin-orbit splittings for various nuclei with closed shells or subshells are also listed in Table I in line with the label "HF + 3N." Comparing the results with those obtained in self-consistent relativistic mean-field calculations also listed in this table (ILDA and $\sigma - \omega$; see discussion above) one finds that the results for ^{16}O and ^{40}Ca, the nuclei with closed major shells, are rather similar. For nuclei with closed subshells, ^{12}C, ^{28}Si, and ^{56}Ni, however, the situation is quite different. While the relativistic mean-field calculations for ^{12}C and ^{28}Si yield positive values for the spin-orbit splitting of the states close to the Fermi energy,
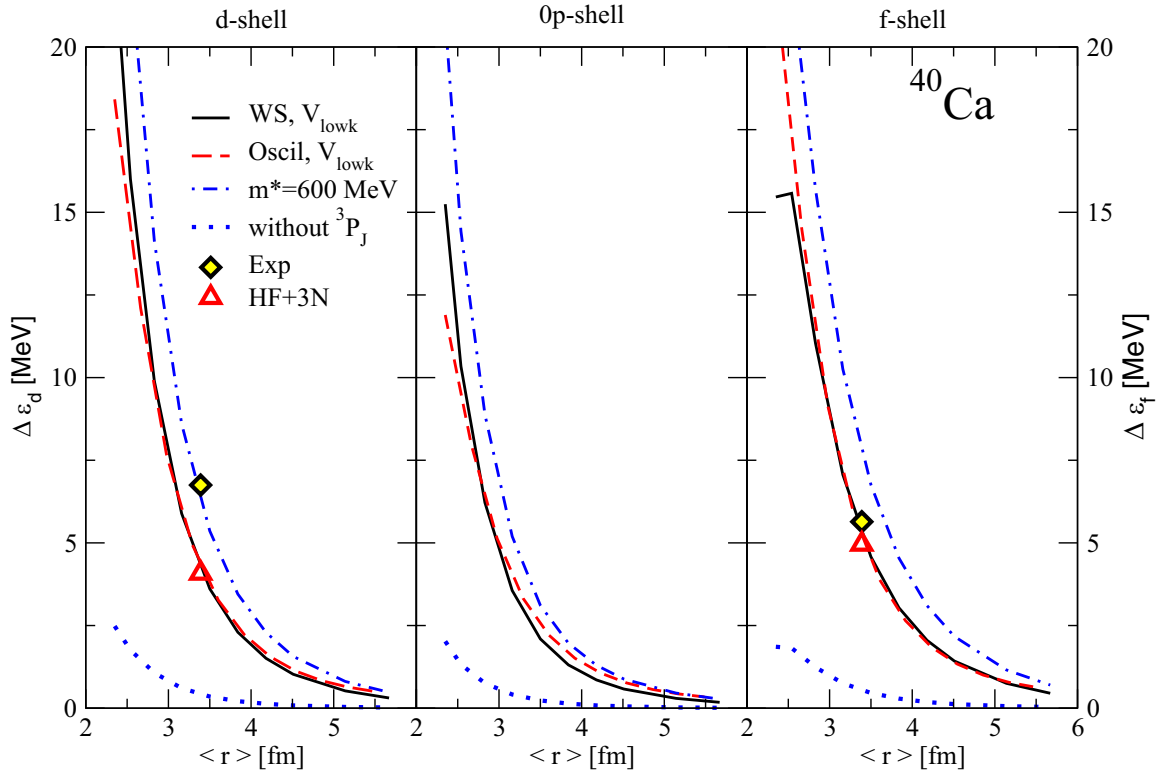
FIG. 5. Results for the spin-orbit splitting in quasinuclear ^{40}Ca are displayed as a function of the radius of the nucleon density distribution $\langle r \rangle$. The left, the middle, and the right panel present results for the splitting in the $0p$ shell, the $0d$ shell, and the $0f$ shell, respectively.

the corresponding results of the nonrelativistic HF + 3N approach yield negative values for the spin-orbit splitting of the p and d shells, respectively. This implies that the assumption of spherical symmetry does not lead to consistent solutions since, e.g., in the case of ^{28}Si, the energy of the unoccupied $d_{3/2}$ shell is below the energy of $d_{5/2}$, which is assumed to be occupied. This implies that deformed solutions or configuration mixing has to be considered to obtain consistent solutions for these nuclei using realistic NN interactions.

The remaining part of this section is devoted to the discussion of the sources within realistic NN interactions causing the spin-orbit splitting in the mean field of nuclei. For that purpose Fig. 6 presents results for the quasinuclear systems of ^{16}O using modifications of the underlying NN interaction. As a reference the black solid lines in this figure correspond to the results obtained for the $V_{\mathrm{low}\,k}$ interaction using the Woods-Saxon wave functions of the nuclear system representing ^{16}O with variable size and are identical to the corresponding results in the left and middle panel of Fig. 4. Now, ignoring the contributions of $V_{\mathrm{low}\,k}$, which originates from partial waves with $L = 1$ for the relative motion and total spin $S = 1$ for the interacting nucleons, i.e., the partial waves $^3P_0$, $^3P_1$, and $^3P_2$, one obtains moderate modifications in the potential energy of the single-particle states, which are around 10% of the total contribution. These partial waves, however, are completely dominating the energy differences, which lead to the spin-orbit splittings. Therefore the results obtained for $V_{\mathrm{low}\,k}$ without the contributions of the ^3P_J partial waves, represented by the red dash-dotted lines in Fig. 6, show results very close to zero.

This result may be used to conclude that the spin-orbit term in the nonrelativistic shell model of the nucleus originates from the spin-orbit structure in the two-nucleon interaction. This spin-orbit structure occurs in partial waves with orbital angular momentum $L \geqslant 1$ and spin $S = 1$. The dominant contribution should occur in the ^3P_J partial waves while the effects in higher partial waves should be smaller due to the finite range of the NN interaction (see also [42]). In fact, this argument has been used, e.g., to justify the origin of the spin-orbit term in simple phenomenological models for the effective NN interaction like the Skyrme force [8], leading to the well-known expression

$$V_{ls}^{\mathrm{Skyrme}}(r) = W \frac{3}{2} \frac{1}{r} \frac{d}{dr} \rho(r), \tag{21}$$

for the leading contribution to the spin-orbit term in the mean-field model for spherical nuclei with a density distribution $\rho(r)$. This analytical form suggests that the strength of the spin-orbit splitting should scale with the size of the nuclear system $\langle r \rangle$ like $\langle r \rangle^{-5}$. Indeed the dependence of the spin-orbit term evaluated from realistic NN interactions, displayed in Figs. 4 and 5, shows this scaling behavior over a wide range of $\langle r \rangle$. It is worth noting that the same scaling behavior is also observed in Figs. 1 and 3, although the results presented in these figures are derived from the relativistic structure of the mean field in nuclear matter.

One of the most important results of relativistic models describing nuclear systems is the feature that a strong scalar component in the mean field of nuclei leads to an
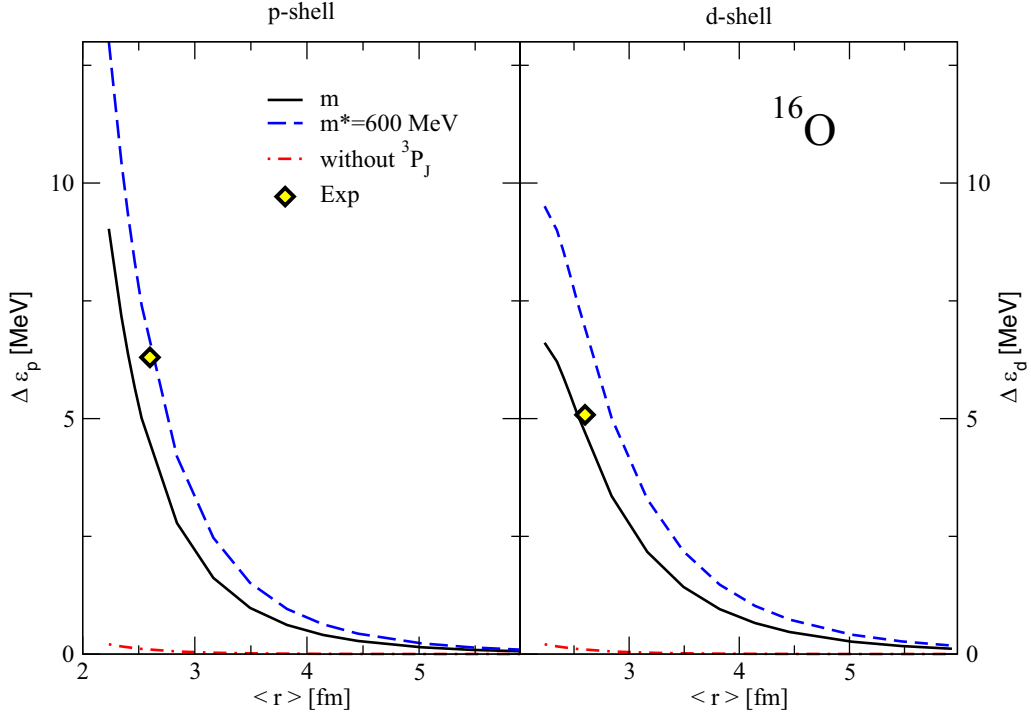
FIG. 6. Results for the spin-orbit splitting in quasinuclear ^{16}O are displayed as a function of the radius of the nucleon density distribution $\langle r \rangle$. The left and the right panel present results for the splitting in the $0p$ shell and the $0d$ shell, respectively. Results obtained for the full $V_{\mathrm{low}\,k}$ are compared to those, where contributions from $^{3}P_J$ partial waves are ignored. The lines with label $m^* = 600$ MeV are obtained evaluating the underlying OBEP with Dirac spinors for the nucleon with enhanced small components.

enhancement of the small component of the Dirac spinor representing the nucleon in the nuclear medium. This feature is represented by an effective Dirac mass m^* for the nucleon, which is smaller than the nucleon mass M in the vacuum. This implies that the matrix elements of a meson-exchange interaction of two nucleons in the nuclear medium should be evaluated for Dirac spinors with a reduced effective mass. In fact, Dirac–Brueckner-Hartree-Fock calculation based on realistic OBE models for the NN interaction have demonstrated that this effect is non-negligible and improves the results of calculations for bulk properties of nuclear matter and finite nuclei considerably [11,23,37,43].

Assuming a realistic value for the Dirac mass in the medium, like, e.g., $m^*c^2 = 600$ MeV, one can calculate the matrix elements of the OBEP A for such Dirac spinors and evaluate a corresponding $V_{\mathrm{low}\,k}$ to represent the effective NN interaction in the nuclear medium [31]. Evaluating the spin-orbit splitting for this effective interaction one obtains the results represented by the blue dashed lines in Fig. 6. Using the same Woods-Saxon wave functions, i.e., the same radius $\langle r \rangle$, an enhancement of the spin-orbit splitting around 30% can be observed (see also [44]).

Rather similar results for this enhancement of the spin-orbit splitting due to the modification of the Dirac spinors as well as the dominance of the $^{3}P_J$ partial waves have also been observed for ^{40}Ca (see Fig. 5).

Since it has been demonstrated above that the results for the spin-orbit term are rather insensitive to the details of the nucleon wave functions, which yield the same radius for the

nucleon distribution, the remaining part of this section will consider oscillator functions, which are easily transformed from the partial waves for relative coordinates, which are used to evaluate the matrix elements for the NN interaction, to oscillator functions in the coordinate system of the nucleus used to determine the properties of the nucleus.

Matrix elements for the oscillator functions with radial quantum number $n = 0$ are displayed in Fig. 7 as a function of the oscillator length:

$$b = \sqrt{\frac{\hbar}{M\omega}}, \qquad (22)$$

with M the mass of the nucleon and ω the oscillator frequency. The various panels show the results for the partial waves $^{3}P_J$, which are relevant for the spin-orbit term in the nuclear shell model, as discussed above. For a comparison also matrix elements in the $^{1}S_0$ channel are given. The matrix elements of the bare OBEP, represented by the black solid line, are rather different from the corresponding results using $V_{\mathrm{low}\,k}$ (red dashed lines) in the $^{1}S_0$ partial wave with orbital angular momentum $L = 0$; the effects of the renormalization leading to $V_{\mathrm{low}\,k}$ are much weaker in the $^{3}P_J$ partial waves. This demonstrates that the renormalization accounts for high-momentum or short-range components of the underlying bare NN interaction, which are strong in the S channel and much weaker in partial waves with $L > 0$.

The results displayed in Fig. 6 also show the effect of the reduced Dirac mass for the nucleons interacting in the nuclear medium by comparing matrix elements of $V_{\mathrm{low}\,k}$ calculated
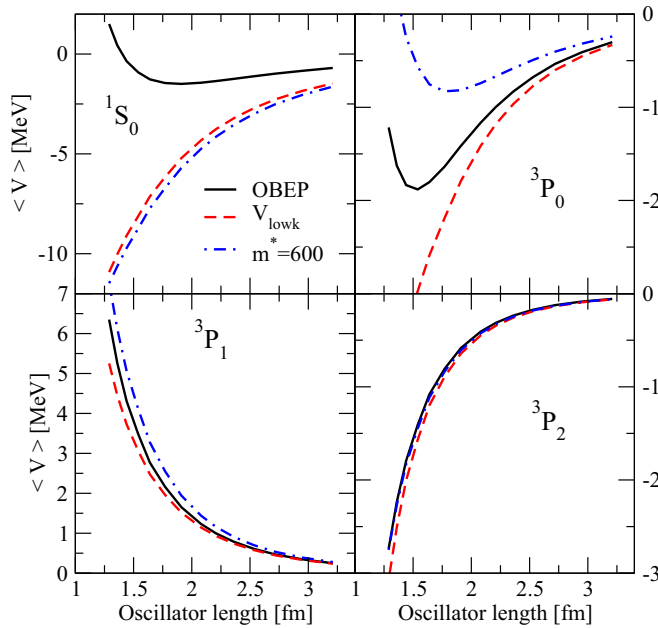
FIG. 7. Results for diagonal matrix elements of the NN interaction, $\langle n = 0|V|n = 0 \rangle$, calculated in an oscillator basis as a function of the oscillator length. The four panels show results in different partial waves for the bare OBEP and the resulting $V_{low\,k}$ interaction. The dash-dotted line (blue) represents results for the low-momentum interactions derived from the OBE potential for Dirac spinors with an effective Dirac mass m^* of $600\,\text{MeV}/\text{c}^2$ with c representing the speed of light.

TABLE II. Spin-orbit splitting for various nuclei with closed shells or subshells calculated within an oscillator model with appropriate oscillator energies $\hbar\omega$ as listed in the first row. For the results displayed in the upper half of this table the OBEP A of [11] has been used, while the results displayed in the lower part are based on the N^{3}LO interaction defined in [12]. All entries are given in MeV.

$\hbar\omega$	^{12}C 16.41	^{16}O 14.02		^{28}Si 11.95	^{40}Ca 10.15		^{56}Ni 9.27
	$0p$	$0p$	$0d$	$0d$	$0f$	$1p$	$0f$
$V_{low\,k}$	-2.92	4.28	6.20	-0.41	4.31	5.26	0.52
BHF	-2.70	4.22	6.13	-0.18	4.24	5.19	0.70
OBEP A	-1.82	4.61	6.79	0.44	5.64	2.54	1.14
$T = 0$	-2.79	-0.02	-0.02	-1.71	0.06	0.03	-1.20
$0.5*(\sigma, \omega)$	-3.89	2.69	4.23	-1.31	3.68	1.78	-0.38
$0.5*\pi$	2.29	4.61	6.51	1.27	5.18	2.18	2.75
N^{3}LO, V	-3.01	4.26	6.16	-0.64	5.19	2.29	0.30
N^{3}LO + 3N, V	-2.37	5.72	7.98	0.21	6.77	2.90	1.17
N^{3}LO, G	-2.81	4.07	5.93	-0.41	4.99	2.20	0.46
N^{3}LO + 3N, G	-2.08	5.34	7.51	0.45	6.34	2.72	1.31

for nucleon spinors of the vacuum to the low-momentum interaction derived from the OBE interaction of nucleons with a Dirac mass $m^*\text{c}^2$ of 600 MeV.

One can see from this figure that the matrix elements are attractive in $^3P_0$ and $^3P_2$ partial waves, whereas repulsive matrix elements are obtained in the $^3P_1$ partial wave. Therefore it is obvious that the interaction in the various ^3P_J channels cannot simply be described in terms of a simple central plus a two-nucleon spin-orbit term. Other nonlocal components, like, e.g., tensor or quadratic spin-orbit terms, are a very important part of a realistic NN interaction.

Assuming oscillator functions the matrix elements displayed in Fig. 6 contribute to the spin-orbit splitting of the $0p$ shell in the nuclear mean field of ^{16}O:

$$\delta\varepsilon_p = 1.125\langle V \rangle_{^3P_0} + 1.6875\langle V \rangle_{^3P_1} - 2.8125\langle V \rangle_{^3P_2}, \quad (23)$$

where $\langle V \rangle_{^3P_J}$ represents the relative oscillator Extracting matrix elements from the corresponding partial wave ^3P_J with radial quantum number $n = 0$. Extracting matrix elements from the corresponding panels of Fig. 6 for an oscillator length, which is appropriate for ^{16}O ($b \approx 1.7$ fm), and applying Eq. (23), one finds that the negative contribution of the $^3P_0$ partial wave is more than compensated by the positive contributions originating from the $^3P_1$ and the $^3P_2$ partial waves, leading to a total value around of 4 MeV, which is very close to the final result.

The individual contributions originating from partial waves with $L = 2$ are non-negligible. The corresponding matrix el-

ement of the $^3D_1$ partial wave yields a contribution to $\delta\varepsilon_p$ of around 0.8 MeV. This energy shift, however, is compensated by the contributions from the other ^3D_J channels, which implies that the value of the spin-orbit splittings in ^{16}O is dominated by the contributions from ^3P_J partial waves (see also Fig. 6).

The contributions of the ^3D_J partial waves become a bit more important in heavier nuclei with closed major shells, but also in ^{40}Ca the ^3P_J contributions are still dominant (see Fig. 5). The situation is rather different in nuclei with closed subshells like ^{12}C, ^{28}Si, or ^{56}Ni. The spin-orbit splittings in these nuclei obtain contributions also from other partial waves like $^1P_1$ or the tensor channel $^3S_1$ - $^3D_1$ (see discussion below).

Results for selected spin-orbit splittings in various nuclei are listed in Table II comparing various approximation schemes for the NN interaction. Since the spin-orbit term is very sensitive to the radius of the nuclear system, the shell-model wave functions have been fixed to oscillator functions, which yield a realistic value for the radius of the nucleus under consideration. The corresponding values for the oscillator frequency, $\hbar\omega$, are listed in the second line of this table.

The lines denoted as $V_{low\,k}$, BHF, and OBEP in the first column of Table II present results of Hartree-Fock calculations assuming $V_{low\,k}$ interaction, Brueckner–Hartree-Fock calculations, and Hartree-Fock calculations assuming the bare OBEP A interaction defined in [11]. Note that these different approaches yield results for the spin-orbit splitting, which are very close to each other, although individual single-particle energies and the total binding energies are rather different in these different approximation schemes. This confirms the finding above: The renormalization effects in $V_{low\,k}$ and BHF to account for effects of short-range correlations have only little influence on the spin-orbit splitting, as the ls term in the nuclear shell model arises from the NN interaction in partial waves with $l = 1$ and larger, which are not very sensitive to the treatment of short-range correlations. Therefore the

subsequent discussion will consider modifications of the bare OBEP.

It is remarkable that all three approaches yield large positive values for the spin-orbit splitting in the closed-shell nuclei ^{16}O and ^{40}Ca, whereas small or negative values are obtained in nuclei with closed subshells. As discussed before, this indicates that the spherical shell model is not applicable in these cases. To explore the origin of this feature, the line in Table II denoted as "$T = 0$" shows the contribution of the NN interaction for pairs of nucleons with isospin $T = 0$. It is evident that the $T = 0$ interaction leads to negligible contributions for the spin-orbit splitting of the closed-shell systems, but provides negative contributions for the spin-orbit splitting of the nuclei with closed subshells. This supports the finding that the deformation of open-shell nuclei mainly originates from the proton-neutron interaction.

Finally, the influence of the various mesons in the OBEP shall be discussed. The line in Table II marked as "$0.5*(\sigma, \omega)$" represents the results obtained with the OBEP quenching the contribution of the scalar σ and the vector ω meson by a factor $1/2$. Compared to the results using the full OBEP one finds a substantial reduction of the spin-orbit splittings.

The matrix elements of the OBEP are most conveniently calculated in momentum space using **q** and **q'** to denote relative momenta for the pair of incoming and outgoing nucleons, respectively. After transforming these expressions using momentum variables of an average relative momentum $\mathbf{p} = 1/2(\mathbf{q} + \mathbf{q'})$ and momentum transfer $\mathbf{k} = (\mathbf{q'} - \mathbf{q})$, one may expand the expressions in terms of $\mathbf{k}^2$ and $\mathbf{q}^2$. This leads to expressions for the NN interaction with a two-body spin-orbit term, which has the same sign for the σ exchange and the ω exchange (see [11,45] for details). It is remarkable that the σ and ω mesons, which lead to contributions of opposite sign for the total energy, provide coherent contributions to the spin-orbit term. This is rather similar to the result obtained in the relativistic mean field [see Eq. (4)].

Table II also shows results using the OBEP, in which the contribution of the π exchange is quenched by a factor $1/2$ (see line with label $0.5 * \pi$). One can see that the π exchange has a negligible influence on the spin-orbit term in the case of the closed-shell nuclei. It yields an attractive contribution in the case of open-shell nuclei, in which the shell with $j = l + 1/2$ is occupied whereas the one with $j = l - 1/2$ is unoccupied. Note that the relativistic mean-field calculations discussed in the first part of this section (see Table I) do not include pion exchange in the NN interaction and yield positive spin-orbit splittings also for open-shell nuclei.

This suppression of the spin-orbit term in open-shell nuclei by the $T = 0$ tensor interaction of a realistic NN interaction has already been observed by Stancu *et al.* [46] in the attempt to include tensor components in the effective Skyrme interaction model. As the inclusion of these tensor components did not improve the results of mean-field calculations they have been ignored for a long time. More recently, $T = 0$ and 1 tensor components in the Skyrme interaction have been adjusted to describe spin-orbit effects in chains of isotopes of spin unsaturated nuclei (see, e.g., [47,48]). Note, however, that the parameters for these effective tensor terms are not deduced from a realistic NN interaction.
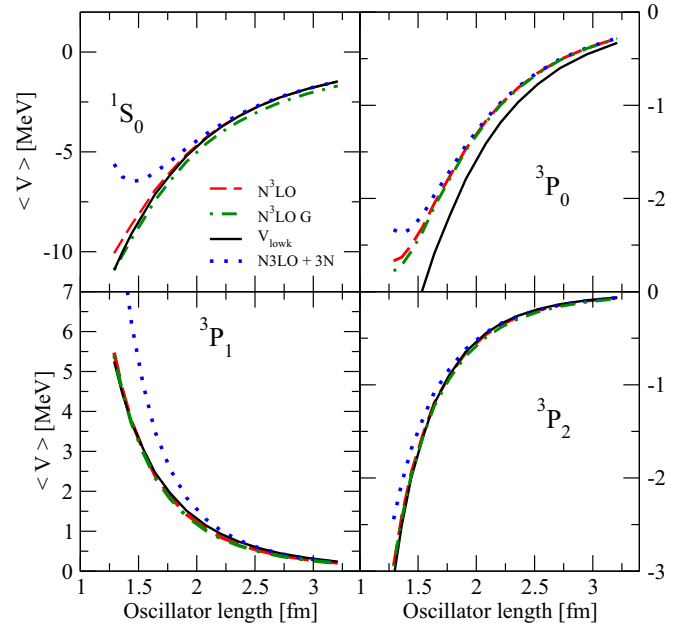

FIG. 8. Results for diagonal matrix elements of the NN interaction, $\langle n = 0|V|n = 0\rangle$, calculated in an oscillator basis as a function of the oscillator length. The four panels show results in different partial waves for the bare N^{3}LO interaction (red dashed line), the corresponding G matrix (green dash-dotted line), and the N^{3}LO interaction including effects of a chiral 3N force expressed in the form of a density-dependent effective NN interaction (blue dotted line). For a comparison also the results of $V_{\mathrm{low}\,k}$ (black solid line) have been copied from Fig. 7.

All calculations discussed so far are based on the meson-exchange model for the NN interaction. For a comparison a realistic NN interaction shall be considered, which has been developed within the framework of chiral effective field theory by Entem *et al.* [12]. They included terms up to fifth order (N^{4}LO) and adjusted the parameter to provide very accurate fits for the NN phase shifts and the data of the deuteron. Here, the model including terms up to fourth order (N^{3}LO) will be considered using a cutoff parameter Λ of 450 MeV, which has also been defined in [12].

In analogy to Fig. 7, Fig. 8 displays oscillator matrix elements in various partial waves. The difference between the the bare N^{3}LO potential (red dashed line) and the corresponding matrix elements of G (green dash-dotted line) is very small even in the $^1S_0$ partial wave, indicating that the interaction is much softer than the OBEP. The agreement between the matrix elements of the bare N^{3}LO interaction and the corresponding G matrix elements is of course even better in the ^3P_J partial waves, which makes it difficult to distinguish between the various lines. This is also reflected by the results for the spin-orbit splitting presented in the lower part of Table II. Results obtained in the Hartree-Fock approach (denoted by N^{3}LO, V) and the Brueckner–Hartree-Fock approach (N^{3}LO, G) are almost identical.

For a comparison Fig. 8 also includes matrix elements of the $V_{\mathrm{low}\,k}$ interaction already displayed in Fig. 7. The agreement between the matrix elements derived from N^{3}LO and

$V_{\text{low }k}$ is good with small deviations in the $^3P_0$ partial wave. The same is true also for the calculated spin-orbit splittings presented in Table II. This demonstrates that nuclear structure calculations using NN interactions, which give a very accurate fit of the NN scattering phase shifts, lead to very similar results for the spin-orbit splitting, if the calculated nuclear radius is the same.

The chiral perturbation expansion also provides a consistent approach for NN and many-nucleon interactions. In fact, 3N interactions are essential to provide a realistic result for the saturation point calculated for infinite nuclear matter. Without such a 3N interaction the chiral NN interactions predict a saturation point of nuclear matter at very high density and very large binding energy, which is typical for soft NN interactions, or no saturation at all. The chiral 3N interaction is usually represented in terms of a density-dependent NN interaction [13,14], taking into account that it originates from a 3N interaction, when the Hartree-Fock mean field is calculated [49,50].

This representation of the chiral 3N interaction in terms of a density-dependent NN interaction has also been used in the present paper to investigate the influence of the chiral 3N interaction on the evaluation of the spin-orbit splitting in finite nuclei. Results for the relevant oscillator matrix elements are also displayed in Fig. 8 (blue dotted lines). Note that the density parameter in the representation of the 3N force has been adjusted to the mean value of the nucleon density distribution in the oscillator model for ^{16}O, using the oscillator length b displayed on the horizontal axis in this figure. This density parameter decreases with increasing b and provides a reason for the fact that the difference between the matrix elements evaluated for N^{3}LO without and with inclusion of the 3N term vanishes with increasing b.

The effect of the 3N interaction is repulsive in all partial waves displayed in Fig. 8. It is large in the $^1S_0$ partial wave, which is irrelevant for the spin-orbit term, and the $^3P_1$ channel. Note that additional repulsion in the $^3P_1$ partial wave enhances the spin-orbit splitting in closed-shell nuclei [see discussion of Eq. (23) above].

Indeed, the results displayed in Table II show a significant enhancement of the spin-orbit splitting for the closed-shell nuclei. In the case of ^{16}O this enhancement improves the agreement with the experimental splitting of 6.3 MeV for the hole states $p_{1/2}$ and $p_{3/2}$. On the other hand, however, the enhancement of the spin-orbit splitting for the particle states ($d_{3/2}$ and $d_{5/2}$) due to the 3N makes the agreement with experiment (5.08 MeV) even worse, as already the results from just NN interaction overestimate this datum.

Here one must notice that the density parameter used in the evaluation of the effective NN interaction has been fixed to a value which corresponds to the mean value of the nuclear density for the nucleus under consideration. This may be appropriate for the spin-orbit splittings of the hole states, but will overestimate the effect for the particle states. For the spin-orbit splitting of the particle states a smaller value for the density parameter would be appropriate or one may even take the limit $\rho = 0$, which means to ignore the effect of the 3N interaction. Also one should keep in mind that

results displayed in Table II approximate the single-particle wave functions by oscillator functions. This is reasonable for the hole states but tends to overestimate the splitting for the particle states (see discussion above).

Note that this density dependence of the NN interaction resulting from a 3N interaction has been used by Nakada and Inakura [51] to motivate a density-dependent spin-orbit term leading to a better description of isotope shifts in Pb nuclei.

In this context it is worth mentioning that also the effects of effective Dirac mass m^*, discussed above, can be considered as a density dependence of the NN interaction or as a 3N force described by the Z diagram with intermediate hole states in the Dirac sea. In the present paper, which aims to explore the qualitative features leading to the spin-orbit splitting, the structure of the Dirac spinors in the nuclear medium has been represented by a global mass parameter. This may be appropriate for the spin-orbit splitting of the hole states and leads to agreement with experiment (see right panel of Fig. 6) whereas for the particle states the assumption $m^* = m$ is preferable and leads to agreement with experiment for the d states (left panel of Fig. 6) [44].

IV. SUMMARY

The aim of this paper has been to explore the occurrence of the spin-orbit term in the mean field of finite nuclei in the transition from infinite nuclear matter to finite nuclei. For that purpose sets of quasinuclear systems have been considered, describing nuclei with closed shells and variable size. Relativistic mean-field calculations as well as nonrelativistic approaches based on realistic models for the NN interaction have been used to determine the spin-orbit splitting in the single-particle spectrum.

One finds a very strong sensitivity of the results on the radius of the nuclear mass distribution. This means that results for the single-particle spectrum of nuclear systems should always be discussed together with the predicted radius. The details of the underlying wave functions are not so important. Eigenfunctions of a Woods-Saxon or oscillator potential as well as self-consistent Hartree-Fock wave functions yield almost identical results if they describe the nucleus with the same radius.

In the framework of relativistic, local mean-field calculations this strong dependence on the size of the system can easily be understood. It is well known that a strong spin-orbit term is obtained from the radial derivative of the difference between the scalar field U_s and the vector field U_0. Since U_s is attractive while U_0 is repulsive they cancel each other to a large extent in calculating binding energies. As the spin-orbit term results from the slope of the difference of U_s and U_0 the potentials add up coherently.

In nonrelativistic mean-field calculations, which are based on NN interactions fitting the NN scattering data, the origin of the spin-orbit term in the nuclear mean field of closed-shell nuclei can be found in the spin dependence of the NN interaction or scattering data. The studies show that the spin-orbit term mainly originates from the NN interaction in partial waves with an orbital angular momentum $L = 1$ for the relative motion and total spin $S = 1$ of the interacting nucleons.

The rules of antisymmetrization require that the nucleons in these ^3P_J partial waves have a total isospin of $T = 1$.

Effects of renormalization of the NN interaction to account for the effects of short-range or high-momentum components are not so important in the partial waves with $L \geqslant 1$ as in those with $L = 0$. This means that calculated single-particle energies are rather different using a bare OBEP or a renormalized interaction as $V_{\mathrm{low}\,k}$ or the Brueckner G matrix, whereas the differences of the energies of spin-orbit doublets are almost identical calculated in terms of OBE, $V_{\mathrm{low}\,k}$, or G in the Brueckner–Hartree-Fock approximation.

The dominance of the partial waves with $L = 1$ and spin of the interacting nucleons $S = 1$ has been used to derive the spin-orbit term in a simple phenomenological model for the effective NN interaction like the Skyrme force [8], leading to an expression which suggests that the strength of the spin-orbit splitting should scale with the size of the nuclear system $\langle r \rangle$ like $\langle r \rangle^{-5}$. Indeed, the dependence of the spin-orbit term evaluated from realistic NN interactions or derived from relativistic mean-field calculations shows this scaling behavior over a wide range of $\langle r \rangle$.

Using the meson-exchange model to describe the NN interaction, one can identify the mesons which are responsible for the spin-orbit term. The spin-orbit term of closed-shell nuclei mainly originates from the exchange of the scalar-isoscalar σ meson and the vector-isoscalar ω meson. The contributions of these two mesons, which provide contributions to the binding energy with opposite sign, add up coherently in the spin-orbit term. This is in line with the observations of the relativistic mean-field approach. It is also in agreement with the analysis of Machleidt [11], who pointed out that an expansion of the OBE amplitudes for σ and ω exchange yields a spin-orbit term in the two-body interaction. This spin-orbit term in the NN interaction could be thought to cause the ls in the nuclear mean field. This line of argumentation is valid only in a rather qualitative way. Matrix elements of realistic NN interactions and phase shifts in the ^3P_J partial waves cannot simply be described in terms of a central and a two-body spin-orbit term.

The analysis of the spin-orbit term is more complicated for nuclear systems with open shells. If a shell with $j = l + 1/2$ is occupied whereas the corresponding one with $j = l - 1/2$ is unoccupied in the spherical shell model, the effects of the interaction in the ^3P_J channels get reduced and counterbalanced by effects of the interaction in the $T = 0$ channel originating to a large extent from pion-exchange amplitudes. Within the spherical mean-field approach this can even lead to negative values for the energy differences between the states

with $j = l - 1/2$ and those with $j = l + 1/2$. This means that the strong proton-neutron interaction favors deformed nuclei in this case.

The results on the spin-orbit term of nuclei discussed so far are not limited to realistic meson-exchange potentials. It turns out that, e.g., a realistic NN interaction derived from chiral perturbation expansion (N^{3}LO defined in [12]) yields almost identical results and one may conclude that nuclear structure calculations using NN interactions, which give a very accurate fit of the NN scattering phase shifts, lead to very similar results for the spin-orbit splitting, if the calculated nuclear radius is the same.

The chiral perturbation theory also provides a consistent description of three-nucleon forces, which are frequently represented in terms of effective density-dependent NN interactions. The spin structure of this effective density-dependent interaction enhances the spin-orbit term considerably. Assuming that the relevant density is smaller for the evaluation of the spin-orbit term for the valence states above the Fermi surface than for the hole states, which are occupied, this can help to improve a simultaneous description of the spin-orbit term for particle and hole states.

The same is true also for the change of the Dirac spinors of the nucleons in the medium described in the framework of the Dirac–Brueckner–Hartree-Fock approach in terms of an effective Dirac mass m^*. This effect can also be understood as an effective three-nucleon interaction described in terms of a medium dependent two-nucleon interaction which enhances the spin-orbit term.

The study of the spin-orbit term of the nuclear mean field presented in this paper has been limited to the case of light nuclei with identical numbers for protons and neutrons ($Z = N$). It may be of interest to extend these studies to heavier nuclear systems to explore the isovector structure of the spin-orbit term more in detail.

ACKNOWLEDGMENTS

[1] P. Ring and P. Schuck, *The Nuclear Many-Body Problem* (Springer-Verlag, Berlin, 1980).

[2] M. Goeppert Mayer, Phys. Rev. **75**, 1969 (1949).

[3] O. Haxel and J. H. D. Jensen, and H. E. Suess, Phys. Rev. **75**, 1766 (1949).

[4] L. Ray, G. W. Hoffmann, and W. R. Coker, Phys. Rep. **212**, 223 (1992).

[5] J. P. Jeukenne, A. Lejeune, and C. Mahaux, Phys. Rev. C **16**, 80 (1977).

[6] G. F. Bertsch and Y. Luo, Phys. Rev. C **81**, 064320 (2010).

[7] H. Müther and A. Polls, Phys. Rev. C **99**, 034315 (2019).

[8] D. Vautherin and D. M. Brink, Phys. Rev. C **5**, 626 (1972).

[9] D. Walecka, Ann. Phys. (NY) **83**, 491 (1974).

[10] B. D. Serot and J. D. Walecka, Adv. Nucl. Phys. **16**, 1 (1986).

[11] R. Machleidt, Adv. Nucl. Phys. **19**, 189 (1989).

[12] D. R. Entem, R. Machleidt, and Y. Nosyk, Phys. Rev. C **96**, 024004 (2017).

[13] J. W. Holt, N. Kaiser, and W. Weise, Phys. Rev. C **79**, 054331 (2009).

[14] J. W. Holt, N. Kaiser, and W. Weise, Phys. Rev. C **81**, 024002 (2010).

[15] H. Müther, A. Polls, and W. H. Dickhoff, Phys. Rev. C **51**, 3040 (1995).

[16] R. Fritz and H. Müther, Phys. Rev. C **49**, 633 (1994).

[17] R. Fritz, Ph.D. thesis, Tübingen University, 1994.

[18] X. Sun, R. Xu, Y. Tian, Z. Ma, Z. Zhang, Z. Ge, H. Zhang, E. N. E. van Dalen, and H. Müther, Phys. Rev. C **101**, 034302 (2020).

[19] E. N. E. van Dalen and H. Müther, Phys. Rev. C **82**, 014319 (2010).

[20] M. Jaminon, Phys. Rev. C **26**, 1551 (1982).

[21] R. Xu, Z. Ma, Y. Zhang, Y. Tian, E. N. E. van Dalen, and H. Müther, Phys. Rev. C **94**, 034606 (2016).

[22] E. N. E. van Dalen and H. Müther, Int. Journ of Mod. Phys. E **19**, 2077 (2010).

[23] R. Brockmann and R. Machleidt, Phys. Rev. C **42**, 1965 (1990).

[24] R. B. Wiringa, R. A. Smith, and T. L. Ainsworth, Phys. Rev. C **29**, 1207 (1984).

[25] K. Erkelenz, Phys. Rep. **13C**, 191 (1974).

[26] K. Holinde and R. Machleidt, Nucl. Phys. A **247**, 495 (1975).

[27] S. K. Bogner, T. T. S. Kuo, and L. Coraggio, Nucl. Phys. A **684**, 432c (2001).

[28] S. K. Bogner, A. Schwenk, R. J. Furnstahl, and A. Nogga, Nucl. Phys. A **763**, 59 (2005).

[29] P. Bozek, D. J. Dean, and H. Müther, Phys. Rev. C **74**, 014303 (2006).

[30] S. K. Bogner, R. J. Furnstahl, S. Ramanan, and A. Schwenk, Nucl. Phys. A **784**, 79 (2007).

[31] E. N. E. van Dalen and H. Müther, Phys. Rev. C **80**, 037303 (2009).

[32] K. Suzuki, Prog. Theoret. Phys. **68**, 246 (1982).

[33] J. Kuckei, F. Montani, H. Müther, and A. Sedrakian, Nucl. Phys. A **723**, 32 (2003).

[34] E. N. E. van Dalen, P. Gögelein, and H. Müther, Phys. Rev. C **80**, 044312 (2009).

[35] N. Kaiser, R. Brockmann, and W. Weise, Nucl. Phys. A **625**, 758 (1997).

[36] R. Machleidt and D. R. Entem, Phys. Rep. **503**, 1 (2011).

[37] H. Müther, F. Sammarucca, and Zhongyu Ma, J. Mod. Phys. E **26**, 173001 (2017).

[38] C. L. Kung, T. T. S. Kuo, and K. F. Ratcliff, Phys. Rev. C **19**, 1063 (1979).

[39] D. Bonatsos and H. Müther, Nucl. Phys. A **496**, 23 (1989).

[40] I. Talmi, Helv. Phys. Acta **25**, 185 (1952).

[41] M. Moshinsky, Nucl. Phys. **13**, 104 (1959).

[42] Y. Y. Sharon, M. S. Fayache, Y. D. Devi, L. Zamick, and H. Müther, Phys. Rev. C **63**, 014303 (2000).

[43] S. H. Shen, H. Z. Liang, J. Meng, P. Ring, and S. Q. Zhang, Phys. Rev. C **96**, 014316 (2017).

[44] L. Zamick, D. C. Zheng, and H. Müther, Phys. Rev. C **45**, 2763 (1992).

[45] R. Machleidt, in *Relativistic Dynamics and Quark-Nuclear Physics*, edited by M. B. Johnson and A. Picklesimer (Wiley, New York, 1986).

[46] F. Stancu, D. M. Brink, and H. Flocard, Phys. Lett. B **68**, 108 (1977).

[47] D. M. Brink and Fl. Stancu, Phys. Rev. C **75**, 064311 (2007).

[48] S. Shen, G. Colo, and X. Roca-Maza, Phys. Rev. C **99**, 034322 (2019).

[49] K. Hebeler and A. Schwenk, Phys. Rev. C **82**, 014314 (2010).

[50] A. Carbone, A. Polls, and A. Rios, Phys. Rev. C **88**, 044302 (2013).

[51] H. Nakada and T. Inakura, Phys. Rev. C **91**, 021302(R) (2015).